Computer Modeling in Engineering & Sciences

Tech Science Press

DOI: 10.32604/cmes.2023.029351

ARTICLE

Flow Breakdown of Hybrid Nanofluid on a Rigid Surface with Power Law Fluid as Lubricated Layers

Mirza Naveed Jahangeer Baig[1], Nadeem Salamat[1], Sohail Nadeem[2,3,*], Naeem Ullah[2], Mohamed Bechir Ben Hamida[4,5,6], Hassan Ali Ghazwani[7], Sayed M. Eldin[8] and A. S. Al-Shafay[9]

[1]Instituite of Mathematics, Khwaja Fareed University of Engineering and Information Technology, Rahim yar Khan, 64200, Pakistan

[2]Department of Mathematics, Quaid-I-Azam University, Islamabad, 44000, Pakistan

[3]Department of Mathematics, Wenzhou University, Wenzhou, 325035, China

[4]College of Engineering, Department of Mechanical Engineering, Imam Mohammad Ibn Saud Islamic University (IMSIU), Riyadh, 11564, Saudi Arabia

[5]Research Laboratory of Ionized Backgrounds and Reagents Studies (EMIR), Preparatory Institute for Engineering Studies of Monastir (IPEIM), University of Monastir, Monastir, 5060, Tunisia

[6]Higher School of Sciences and Technology of Hammam Sousse, Department of Physics, Jazan, 82511, Kingdom of Saudia Arabia

[7]Department of Mechanical Engineering, Faculty of engineering, Jazan University, P. O. Box 45124, Jazan, Kingdom of Saudia Arabia

[8]Center of Research, Faculty of Engineering, Future University in Egypt, New Cairo, 11835, Egypt

[9]Department of Mechanical Engineering, College of Engineering, Prince Sattam bin Abdulaziz University, Alkharj, 16436, Saudi Arabia

*Corresponding Author: Sohail Nadeem. Email: sohail@qau.edu.pk

Received: 14 February 2023 Accepted: 14 June 2023 Published: 17 November 2023

ABSTRACT

This work investigates an oblique stagnation point flow of hybrid nanofluid over a rigid surface with power law fluid as lubricated layers. Copper (Cu) and Silver (Ag) solid particles are used as hybrid particles acting in water H_2O as a base fluid. The mathematical formulation of flow configuration is presented in terms of differential system that is nonlinear in nature. The thermal aspects of the flow field are also investigated by assuming the surface is a heated surface with a constant temperature T. Numerical solutions to the governing mathematical model are calculated by the RK45 algorithm. The results based on the numerical solution against various flow and thermal controlling parameters are presented in terms of line graphs. The specific results depict that the heat flux increases over the lubricated-indexed parameter.

KEYWORDS

Oblique stagnation point flow; hybrid nanofluid; lubricated layer; magnetohydrodynamics

This work is licensed under a Creative Commons Attribution 4.0 International License, which permits unrestricted use, distribution, and reproduction in any medium, provided the original work is properly cited.

Nomenclature

Symbols	Description	Dimensions
T_w, T_∞	Temperature field	$[K]$
μ_r	Coefficient of viscous effect	K
Pr	Prandtl number	Pr
λ	Lubrication parameter	_
α_{hnf}	Thermal diffusivity (hybrid model)	_
$\alpha_{s1}, \alpha_{s2}, \alpha_f$	Thermal diffusivity (nanoparticle Ag, Cu and water)	_
σ_{hnf}	Electrical conductivity of nanofluids	_
ν_{hnf}	Kinematic viscosity (hybrid nanofluid)	_
ν_f, ν_s	Kinematic viscosity (water and nanoparticles)	_
k_{hnf}	Thermal conductivity (hybrid model)	_
k_{s1}, k_{s2}, k_f	Thermal conductivity (nanomaterials and water)	_
$(\rho C_p)_{hnf}$	Heat capacitance (hybrid model)	_
ρ_{hnf}	Density of hybrid nanofluids	_
H_0	Magnetic field component	
$\rho_f, \rho_{s1}, \rho_{s2}$	Density of base fluid and solid fraction	
$\overline{u}, \overline{v}$	Velocity components	u, v
$\overline{p}$	Pressure	P
$\overline{\psi}$	Stream function	ψ
$\overline{f}(\overline{y})$	Normal component of the flow	$f(y)$
$\overline{x}, \overline{y}$	Spatial coordinates	x, y
$\overline{p}$	Pressure field	P
T	Temperature field	$\theta(y)$
M	Hartman number	_

1 Introduction

Nanofluids are believed to be an integral part of nanotechnology. In many industrial sectors and manufacturing procedures, exchangers for heat are used because of the nanofluid's ability to exceed the same degree of heat transfer and thermal conductivity as typical fluids such as water, kerosene and ethylene glycol. They are utilized as underlying fluids since they have a low viscosity level, density, and thermal conductivity. In many engineering fields and manufacturing processes, efficient heat transfer is required. This includes polymer extraction procedures, paper production, residential cooling, nuclear reactors, the polymer sector, lubricant manufacturing, and food processing. Employing ultrafine nanometer particles in manufacturing (base) solutions may boost thermal properties. The kinds of nanoparticles comprise metals (Cu, Al, Fe, Ag), metal oxides, carbides (Silicon carbide, Titanium carbide), and nonometals (SWCNT and MWCNT). The thermal conductivity of a great deal of industrial fluids (base fluids), such as kerosene oil, grease, motor oil, propylene glycol and ethylene glycol etc., is incredibly low. Masuda et al. supplied the initial proposal for dispersing nanomaterials in the base liquid [1]. Choi et al. [2] later came up with the phrase "nanofluid." Systems based on nanofluids have applications in a wide range of industries, including heat exchangers, solar collectors, automotive cooling, nuclear reactor cooling, and electronic cooling. Hybrid nanofluid, a mixture of two different types of nanoparticles, has been the focus of several experiments [3,4]. But these types of

hybrid nanoparticles are used to increase thermal conductivity as compared to nanofluid. Riaz et al. [5] executed the computational study for hybrid nanofluids with heat exchangers. Khan et al. [6] studied fundamental aspects of hybrid nanomaterial-confined yaw cylinders. For a hybrid nanofluid issue induced by a slanted spinning disc, Acharya [7] used spectral quasi-linearization numerical methods. In contrast with nanoparticles, hybrid nanofluids improved the rate of transmission of heat at the surface, according to Suresh et al.'s [8] research. The contact of fluid with solid objects creates stagnation points. Near the point of stagnation, the flow manifests maximal levels of heat transmission, static push, and mass discharge. Stagnation flows are essential for friction reduction, transpiration cooling (such as cooling a nuclear activator), some hydraulic and industrial operations. Weidman [9] thoroughly explored the hybrid nanofluid non-axisymmetric thermal potential. The flow and heat transfer examinations of nanofluid at the stagnation point on an exponentially surface affected by a magnetic field were covered by Ur Rehman et al. [10]. When a fluid strikes a surface obliquely at any angle of occurrence, oblique stagnation point flow occurs. An aircraft wing or blood flow at the intersection of the anterior cerebral artery (ACA) and the anterior communicating artery are both instances of such flows. Yuan et al. [11] scrutinised the effect of mixed convection on the flow of viscous fluid near an oblique stagnation point. The slip boundary circumstance for rotating fluid stagnation point flow via power law lubricant was identified by Andersson [12]. Recently, scientists conducted research into heat transmission in non-Newtonian stagnation point flow via lubricant sheets. The benefits of lubricated surface over oblique stagnation point flow of second-grade fluid with mass and heat flux have been investigated by Abbasi et al. [13] for hydraulic systems. Nadeem et al. [14] discovered the effects of a lubricated surface on a micropolar fluid's oblique stagnation point flow. The unique type of flow was initially developed by Wang [15] by extending the sheet. Analysing MHD has fundamental significance for manufacturing, structure, and material investigations. It is greatest significance during the period related to drug discontinuation, asthma cure, cancer treatments, and generator intensity. Some recent research articles that address the topic of MHD flow inside a porous medium with irreversibility analysis and the influence of unsteadiness and Brownian flux on boundary extent are referred to as [16–18]. The above literature exhibits the study of nanofluids and orthogonal stagnation flows under various configurations. There is still no solution for the oblique stagnation flow using Casson fluid with MHD over the lubricant surface. We will find solutions. A hybrid nanofluid studied over a lubricated surface is considered in this evaluation, influenced by the magnetic effect. BVP [mid-rich] on the Maple platform is used to address numerically the simulated flow problem. Graphs and tables are used to demonstrate the results for each of the parameters without dimensions and to provide an appropriate explanation. By comparing our results to previous publications, we were able to figure out that all our findings were in excellent agreement, proving the accuracy of our research.

2 Problem Formulation and Governing Equations

Fig. 1 considers an incompressible, non-Newtonian Casson hybrid nanofluid flowing steadily as it orthogonally impacts an endless number of lubricated surfaces in the xy-plane. The fluid is placed in the upper half of plan y ≥ 0. Casson fluid tensor stress is as follows [19]:

$$\tau_{ij} = -P_{ij} + \begin{Bmatrix} 2\left[\mu_B + \dfrac{P_y}{\sqrt{2\pi}}\right] e_{ij}\pi > \pi_c \\ 2\left[\mu_B + \dfrac{P_y}{\sqrt{2\pi}}\right] e_{ij}\pi < \pi_c \end{Bmatrix}$$

where $\pi = e_{ij}e_{ij}$ and e_{ij}, (i, j) are deformation rate components, π represents the deformation rate, π_c shows critical value. Whereas μ_B exhibits viscosity parameter. P_y is stress of the fluid slurry. Power law fluid flow rate Q is restricted as given below:

$$Q = \int_0 \overline{U}\,(x, y)\,dy$$

$$\mathrm{Q} = \int_0^{\overline{H}} \overline{U}\,(\mathrm{x}, \mathrm{y})\ \mathrm{dy}$$

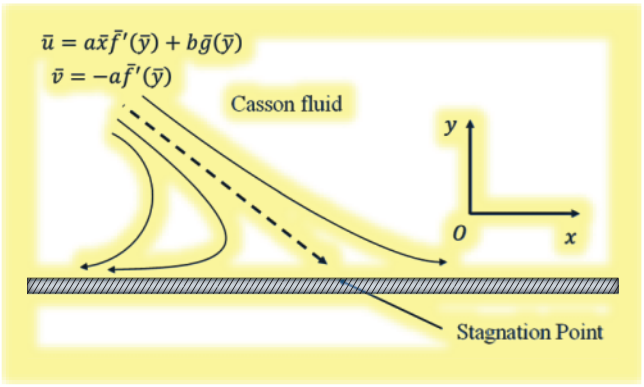

Figure 1: Geometrical description of the issue

A 2-D Oblique stagnation point flow is investigated past a power law fluid lubricated surface with magnetohydrodynamic (MHD) effects. Under this assumption the governing equation are as follows [20]:

$$\frac{\partial \overline{\mathrm{u}}}{\partial \overline{\mathrm{x}}} + \frac{\partial \overline{\mathrm{u}}}{\partial \overline{\mathrm{y}}} = 0 \tag{1}$$

$$\overline{u}\frac{\partial \overline{u}}{\partial \overline{\mathrm{x}}} + \overline{v}\frac{\partial \overline{u}}{\partial \overline{\mathrm{y}}} = -\frac{\partial p}{\rho_{hnf}\partial \overline{\mathrm{x}}} + \nu_{hnf}\left(1 + \frac{1}{\beta}\right)\left(\frac{\partial^2 \overline{u}}{\partial \overline{\mathrm{x}}^2} + \frac{\partial^2 \overline{u}}{\partial \overline{\mathrm{y}}^2}\right) - \frac{4a^2\sigma_{hnf}{B_0}^2\overline{u}}{\rho_{hnf}\,(4a^2 + b^2)}, \tag{2}$$

$$\overline{u}\frac{\partial \overline{v}}{\partial \overline{\mathrm{x}}} + \overline{v}\frac{\partial \overline{v}}{\partial \overline{\mathrm{y}}} = -\frac{\partial p}{\rho_{hnf}\partial \overline{\mathrm{y}}} + \nu_{hnf}\left(1 + \frac{1}{\beta}\right)\left(\frac{\partial^2 \overline{v}}{\partial \overline{\mathrm{x}}^2} + \frac{\partial^2 \overline{v}}{\partial \overline{\mathrm{y}}^2}\right) - \frac{4a^2\sigma_{hnf}{B_0}^2\overline{v}}{\rho_{hnf}\,(4a^2 + b^2)}, \tag{3}$$

$$\overline{u}\frac{\partial \overline{T}}{\partial \overline{\mathrm{x}}} + v\frac{\partial \overline{T}}{\partial \overline{\mathrm{y}}} = \alpha_{hnf}\left(\frac{\partial^2 \overline{T}}{\partial \overline{\mathrm{x}}^2} + \frac{\partial^2 \overline{T}}{\partial \overline{\mathrm{y}}^2}\right), \tag{4}$$

The boundary condition are

$$\overline{u}\,(x, 0) = 0, \quad \overline{v}\,(\overline{\mathrm{y}}, 0) = 0, \quad \overline{v}\,(\overline{x}, \overline{y_1}) = 0, \quad \forall \quad \overline{y_1} \in [0, \delta\,(x)]\,,$$

$$\overline{T} = T_W \text{ at } y = 0, \quad \overline{T} = T_\infty \text{ as } y = \infty. \tag{5}$$

The impinging velocity will not distribute owing to power law fluid their vertical velocity is always zero.

where μ_L is the viscosity of lubrication, then

$$\mu_{hnf}\left(1+\frac{1}{\beta}\right)\frac{d\overline{u}}{dy}=\mu_L\frac{d\overline{U}}{dy} \tag{6}$$

Suppose that $\frac{d\overline{U}}{dy}\ll\frac{d\widehat{U}}{dy}$ then μ_L can be composed as

$$\mu_L=k^*{}_1\left(\frac{d\widehat{U}}{dy}\right)^{n-1} \tag{7}$$

where $k^*{}_1$ and n are coefficient of viscosity and flow behavior index of lubricant, respectively.

Let be velocity components which is given below is used to convert PDEs into ODEs:

$$\begin{aligned}\overline{u}&=a\overline{x}\overline{f}'(\overline{y})+b\overline{g}(\overline{y})\\ \overline{v}&=-a\overline{f}(\overline{y})\end{aligned} \tag{8}$$

$$\overline{H}_0=\frac{B_0}{\sqrt{4a^2+b^2}}\left(-b\hat{i}+2a\hat{j}\right) \tag{9}$$

Here some constant values are a, b and MHD field effect is H_0.

$$\mu_{nf}=\frac{\mu_f}{(1-\varphi)^{2.5}\left[(1-\varphi)\rho_f+\varphi\rho_s\right]},\quad \rho_{nf}=(1-\varphi)\rho_f+\varphi\rho_s,\quad \nu_{nf}=\frac{\mu_f}{\left[(1-\varphi)\rho_f+\varphi\rho_f\right](1-\varphi)^{2.5}},$$

$$\left(\rho C_p\right)_{nf}=(1-\varphi)\left(\rho C_p\right)_f+\varphi\left(\rho C_p\right)_s,\quad \frac{k_{nf}}{k_f}=\frac{\left(k_s+2k_f\right)-2\varphi\left(k_f-k_s\right)}{\left(k_s+2k_f\right)+\varphi\left(k_f-k_s\right)},\quad M=\frac{4a^2\sigma_{hnf}\mathrm{B}_0{}^2}{4\mathrm{a}^2+\mathrm{b}^2},$$

$$Pr=\frac{\nu_f}{k_f},\quad \xi=\sqrt{\frac{a}{\nu_f}}y,\quad \nu_{nf}=\frac{\mu_f}{\left[(1-\varphi)\rho_f+\varphi\rho_f\right](1-\varphi)^{2.5}}, \tag{10}$$

using above velocity component, we got these results which are below:

$$\nu_{hnf}\left(1+\frac{1}{\beta}\right)\overline{f}^{(iv)}+a\overline{f}\,\overline{f''}-a\overline{f'}\,\overline{f''}-\frac{4a\mathrm{B}_0{}^2\sigma_{hnf}\overline{f''}}{(4a^2+b^2)\rho_{hnf}}=0, \tag{11}$$

$$\nu_{hnf}\left(1+\frac{1}{\beta}\right)\overline{g'''}+a\left(\overline{f}\,\overline{g''}-\overline{g}\,\overline{f''}\right)-\frac{4a\sigma_{hnf}\mathrm{B}_0{}^2\overline{g'}}{(4a^2+b^2)\rho_{hnf}}=0, \tag{12}$$

After taking integration of Eqs. (11) and (12), we get

$$\frac{\nu_{hnf}}{a}\left(1+\frac{1}{\beta}\right)\overline{f'''}+\overline{f''}\,\overline{f}-\overline{f'}^2+\frac{4a\sigma_{hnf}\mathrm{B}_0{}^2\left(1-\overline{f'}^2\right)}{(4a^2+b^2)\rho_{hnf}}+1=0, \tag{13}$$

$$\frac{\nu_{hnf}}{a}\left(1+\frac{1}{\beta}\right)\overline{g''}+\overline{f'}\,\overline{g}-\overline{f}\,\overline{g'}-\frac{4a\sigma_{hnf}\mathrm{B}_0{}^2(g-y+\beta)}{(4a^2+b^2)\rho_{hnf}}+(\beta-\alpha)=0, \tag{14}$$

Boundary condition of above Eqs. (13) and (14) becomes (15) below here:

$$\overline{f}'(\infty)=1,\quad \overline{g'}(\infty)=1,\quad \overline{f}(\infty)=\overline{y}-A,\quad \overline{g}(\infty)=\overline{y}-B, \tag{15}$$

With the help of similarty transformation, we changed into a dimensionless equation:

$$y = \overline{y}\sqrt{\frac{a}{v_f}}, \quad f(y) = f(\overline{y})\sqrt{\frac{a}{v_f}}, \quad g(y) = g(\overline{y})\sqrt{\frac{a}{v_f}}, \quad T = \frac{\overline{T} - T_\infty}{T_W - T_\infty}. \tag{16}$$

We got these Diemensional ODE's (17−19) from above using similarty trasnformation:

$$\frac{v_{hnf}}{vf}\left(1 + \frac{1}{\beta}\right)f''' + ff'' - f'^2 + \frac{M^2\frac{\sigma_{hnf}}{\sigma_f}(1 - f')}{\frac{\rho_{hnf}}{\rho_f}} + 1 = 0, \tag{17}$$

$$\frac{v_{hnf}}{vf}\left(1 + \frac{1}{\beta}\right)g'' + (fg' - f'g) - \frac{M^2\frac{\sigma_{hnf}}{\sigma_f}(g - y + \beta)}{\frac{\rho_{hnf}}{\rho_f}} - (\beta - \alpha) = 0, \tag{18}$$

$$\frac{\alpha_{hnf}\theta''}{p_r} + f\theta' = 0, \tag{19}$$

Boundary conditions are as follows:

$$\left(1 + \frac{1}{\beta}\right)f''(0) = \frac{\mu_f}{\mu_{nf}}\lambda(f'(0))^{2n}, \tag{20}$$

$$\left(1 + \frac{1}{\beta}\right)f'(0) = \frac{\mu_f}{\mu_{nf}}\lambda(f'(0))^{2n-1}g(0), \tag{21}$$

$$\lambda = \frac{\sqrt{v_f}x^{2n-1}a^{2n}}{\mu_f a^{\frac{3}{2}}(2Q)^n}, \tag{22}$$

$$\theta(0) = 1, \quad \theta(\infty) = 0, \quad g(\infty) = y - \beta, \quad f(\infty) = y - \alpha, \quad f(0) = 0, \quad f'(\infty) = 1. \tag{23}$$

The formulas for C_f and Nu are

$$C_f = \frac{\tau_w}{\frac{1}{2}\rho_f U_w^2}, \quad Nu = \frac{xq_w}{k_f\left(\overline{T}_w - \overline{T}_\infty\right)}, \tag{24}$$

where τ_w, q_w are local wall shear stress and the surface heat flux defined by

$$\tau_w = \left[\left(\mu_{nf} + \mu_r\right)\frac{\partial\overline{u}}{\partial\overline{y}} + \mu_r\overline{N}\right]\Bigg|_{\overline{y}=0}, \quad q_w = -k_{nf}\left.\frac{\partial\overline{T}}{\partial\overline{y}}\right|_{\overline{y}=0}, \tag{25}$$

by using Eq. (8), the dimensionless values of C_f and Nu are

$$C_f = \frac{2\left(\mu_{hnf}\right)\sqrt{Re}f'' + \frac{bg'}{a}}{\sqrt{Re}\mu_f}, \quad Nu = -\frac{k_{hnf\theta'(0)}}{k_f}, \tag{26}$$

3 Numerical Method Explanation

Employing the Maple BVP [mid-rich] command with the option numeric, the set of nonlinear ordinary differential Eqs. (17)–(19) combining boundary Eqs. (20)–(23) has been solved numerically.

The 4,5 order Rung-Kutta Fehlberg approach for solving issues with boundary values was automatically found by this software.

The RK 45 uses 4th and 5th order Rung-kutta scheme. The used algorithm is as follows:

$$l_o = f\left(x_j, y_j\right) h,$$

$$l_1 = f\left(x_j + \frac{h}{4}, y_j + \frac{l_0}{4}\right) h,$$

$$l_2 = f\left(x_j + \frac{3h}{8}, y_j + \frac{3l_0}{32} + \frac{9l_1}{32}\right) h,$$

$$l_3 = f\left(x_j + \frac{12h}{13}, y_j + \frac{1932l_0}{2197} - \frac{7200l_1}{2197} + \frac{7296l_2}{2197}\right) h,$$

$$l_4 = f\left(x_j + h, y_j + \frac{439l_0}{216} - 8l_1 + \frac{3680l_2}{513} - \frac{845l_3}{4104}\right) h,$$

$$l_5 = f\left(x_j + \frac{h}{2}, y_j - \frac{8l_0}{27} + 2l_1 - \frac{3544l_2}{2565} + \frac{1859l_3}{4104} - \frac{11l_4}{40}\right) h,$$

$$y_{i+1} = y_j - \frac{8l_0}{27} + 2l_1 - \frac{3544l_2}{2565} + \frac{1859l_3}{4104} - \frac{11l_4}{40},$$

$$y_{j+1} = y_j + \frac{25l_0}{216} + \frac{1408l_2}{2565} + \frac{2197l_3}{4104} - \frac{l_4}{5},$$

$$z_{j+1} = z_j + \frac{16l_0}{135} + \frac{6656l_2}{12825} + \frac{28561l_3}{56430} - \frac{9l_4}{5} + \frac{2l_5}{55}.$$

4 Results and Discussion

In this portion, we used excellent Maple packages and BVP [mid-rich] tackles for examining the system of nonlinear differential Eqs. (17) to (19). The BVP [mid-rich] methodology uses mathematics to tackle boundary value constraints. To explain how physical, non-dimensional characteristics like the Casson parameter β, the magnetic field variable and the Prandtl number Pr effect nonlinear ODEs, The Pr value determines the relative thickness of the momentum and thermal boundary extents in heat transfer problems. Thus, for liquid metals, the temperature boundary layer is much thicker than the velocity boundary layer. Lubricated parameter λ are examined by graphical representation. The results of pertinent physical parameters on velocity profile $f'(\eta), g'(\eta)$ and temperature $\theta(\eta)$ are highlighted in this part through graphics. Fig. 2 is developed to examine the behaviour of $f(\eta)$, $f'(\eta)$ *and* $f''(\eta)$. $f''(\eta)$ which is decreasing and gets its minimum value at the boundary. It is maximum at $\eta = 0$ and minimum at $\eta = 5$. When the Hartmann number M is increased, the velocity profile f' increases. The Hartmann number M is the ratio of electromagnetic force to viscous force. It decreases convective heat transfer and fluid velocity. At higher Hartmann numbers M, the magnetic field represents fluid flow, and conduction becomes the predominant mechanism of heat transfer. When we increase Hartmann numbers M, heat transfer modes in MHD fluids gradually change from conduction to convection. When Hartmann number M decreases, it reduces the boundary layer and magnitude of the velocity profile. In Fig. 3, when we increase Hartmann number, its velocity increases.

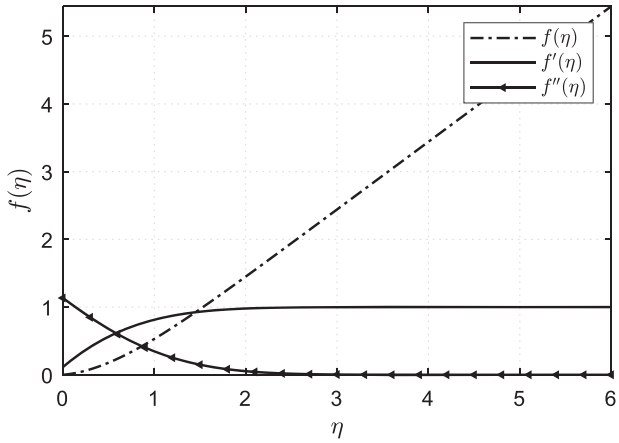

Figure 2: $f(\eta)$ behavior over the values of η

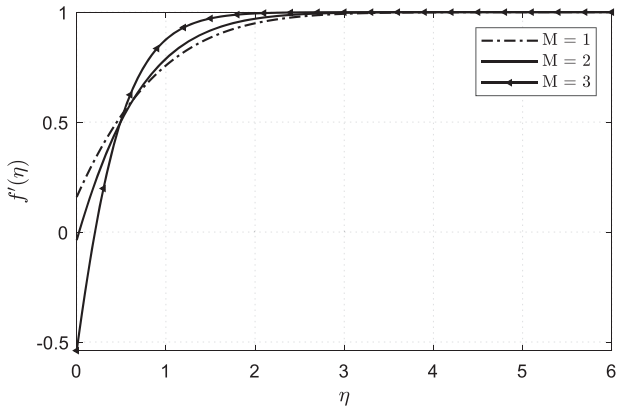

Figure 3: $f'(\eta)$ for $\beta = 4, \mathrm{Pr} = 6.2$

In Fig. 4, when the value of Hartmann number M increases and $\beta = 4$, the value of f(η) will decrease. In Fig. 5, variation of Hartmann number M in increasing order at constant lubrication parameter $\lambda = -2$ and Casson parameter $\beta = 4$. Lubrication parameter λ constant means direct impact on the thickness of the oil film is constant because lubricant parameter is used to find viscosity and coefficient describing the dependence of viscosity on temperature and pressure. Figs. 6–9 show that when the Hartmann number M is increased but the Casson parameter $\beta = 4, 0, -4$ is varied, the velocity profile $g'(\eta)$ increases. The velocity field reduced when the Casson parameter β values grow. However, the temperature rises as the Casson parameter β rises. In Fig. 10, we increase the Casson parameter $\beta = 1, .6, .36$ then it is also decreasing $g'(\eta)$. When we increase the Casson parameter β, its temperature and thermal diffusivity are increasing. Infinity is a large value of the Casson parameter β, and our problem becomes a Newtonian fluid. Higher values of the Casson parameter β produce resistance in fluids, and the thickness of the boundary layer reduces. Fig. 11 shows that the velocity profile g(η) is decreasing when we increase the Hartmaan number from M = 0.4, 0.7, and 0.9. When other parameters are constant. Temprature $\theta(\eta)$ profile in Fig. 12 Hartmaan number M increases from 0.5 to 4.5, at $\beta_1 = -4$ which temperature Profile $\theta(\eta)$ will decrease. We compared our results, and a good agreement is found between present and current results in Table 3. Table 1 presents "Thermo Physical characteristics of hybridnanofluid" and Table 2 describes "Thermo Physical properties of

nanoparticles and base fluid", respectively, are used to Present graphs and help us to find numerical solution in maple BVP [mid-rich].

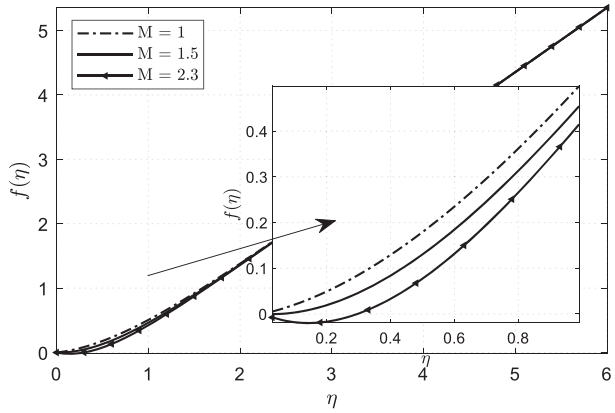

Figure 4: Plots showing $f(\eta)$ for $\beta = 2, \lambda = -4$ and $\alpha = 0.6765$

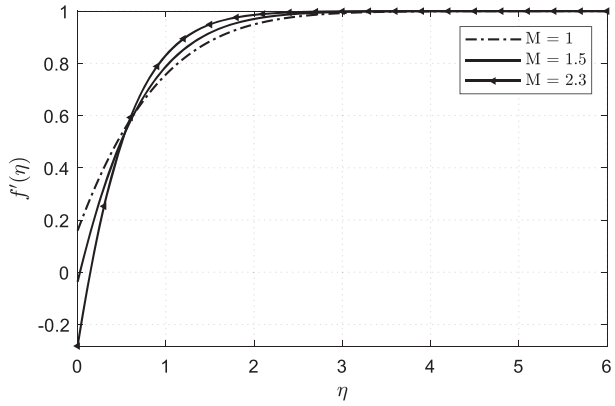

Figure 5: Plots showing $f'(\eta)$ for $\beta = 2, \beta_1 = -4$ and $\alpha = 0.6765$

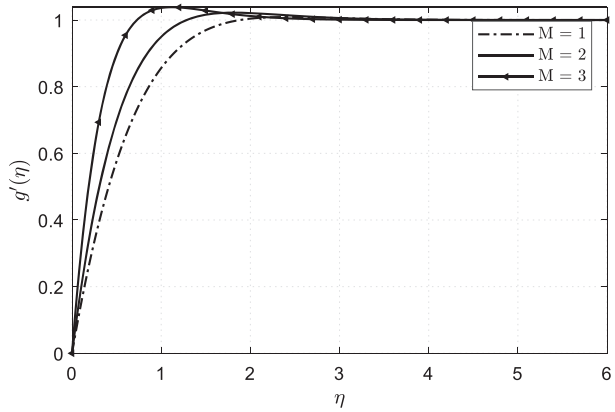

Figure 6: Plots showing $g'(\eta)$ for $\beta = 4, \beta_1 = 2$ and $\alpha = 0.6765$

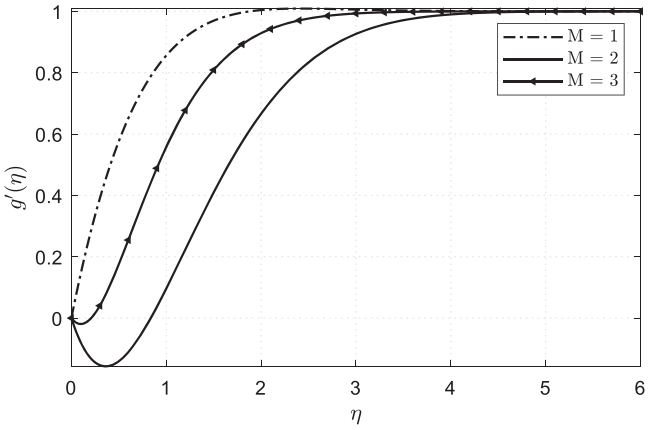

Figure 7: Plots showing $g'(\eta)$ for $\beta = -4, n = 0, \lambda = 0.2, \beta_1 = 2$ and $\alpha = 0.6765$

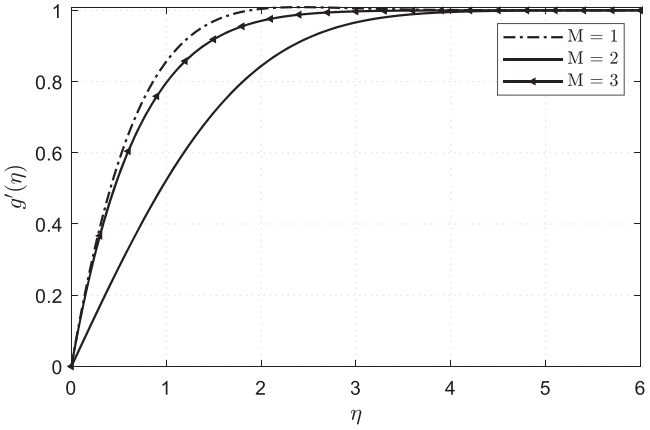

Figure 8: Plots showing $g'(\eta)$ for $\beta = 0, n = 0, n = 0, \lambda = 0.2$ and $\alpha = 0.6765$

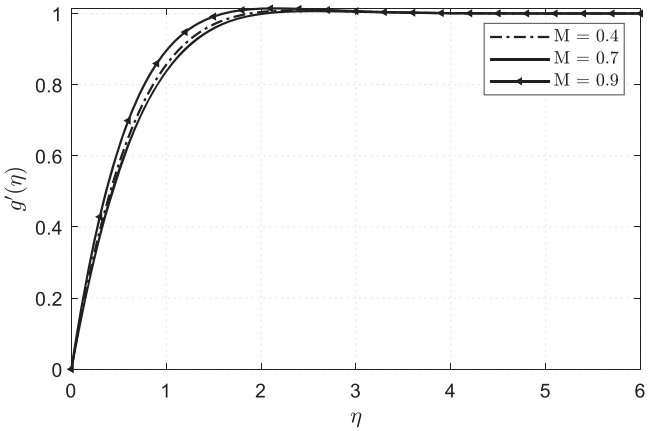

Figure 9: Plots showing $g'(\eta)$ for $\beta = 2, \beta_1 = 4, \lambda = 0.2, \alpha = 0.6765$ and $n = 0.5$

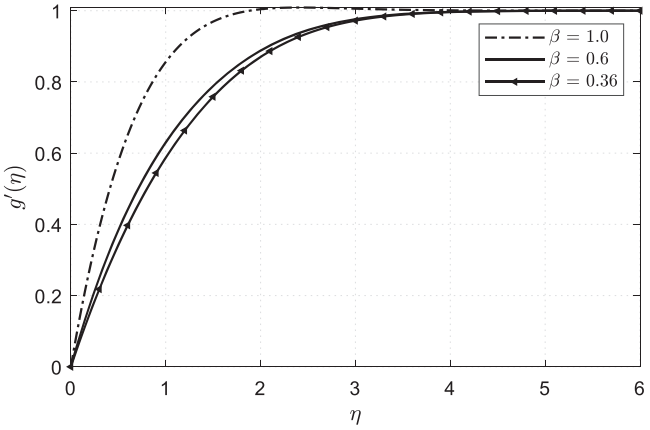

Figure 10: Plots showing $g'(\eta)$ for $M = 1, \beta_1 = 0, \lambda = 0.2, n = 0.2$ and $\alpha = 0.6765$

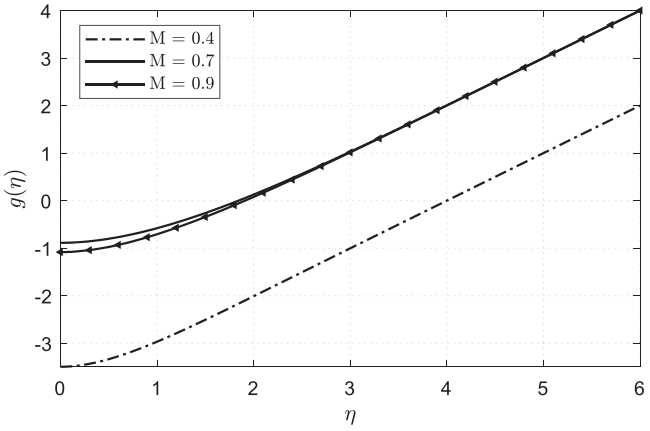

Figure 11: Plots showing $g(\eta)$ for $\beta = 2, \beta_1 = 4, \alpha = 0.6765, \lambda = 0.2$ and $n = 0.5$

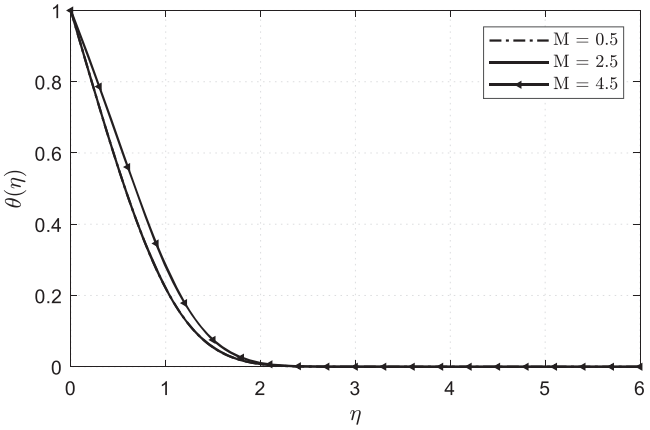

Figure 12: Plots showing $\theta(\eta)$ for $M = 0.5, 2.5, 4.5, \beta = 2, \beta_1 = -4$ and $\alpha = 0.6765$

Table 1: Thermo-physical characteristics of Hybride nanofluid [21,22]

Hybrid nanofluid
$\mu_{hnf} = \dfrac{\mu_f}{\left[\left(1-\varphi_{s1}\right)\left(1-\varphi_{s2}\right)\right]^{2.5}}$
$\rho_{hnf} = \left[\left(1-\varphi_{s2}\right)\left\{\left(1-\varphi_{s1}\right)\rho_f + \varphi_{s1}\rho_{s1}\right\} + \varphi_{s2}\rho_{s2}\right.$
$(\rho_{C_p})_{hnf} = [(1-\varphi_{s2})\{(1-\varphi_{s1})(\rho_{C_p})_f + \varphi_{s1}(\rho_{C_p})_{s1}\}] + \varphi_{s2}(\rho_{C_p})_{s2}$
$\left[\left[\dfrac{\left(\dfrac{k_{s1}\varphi_{s1}+k_{s2}\varphi_{s2}}{(\varphi_{s1}+\varphi_{s2})} + 2k_f + 2\left(k_{s1}\varphi_{s1}+k_{s2}\varphi_{s2}\right) - 2k_f\left(\varphi_{s1}+\varphi_{s2}\right)\right)}{\left(\dfrac{k_{s1}\varphi_{s1}+k_{s2}\varphi_{s2}}{(\varphi_{s1}+\varphi_{s2})} + 2k_f - \left(k_{s1}\varphi_{s1}+k_{s2}\varphi_{s2}\right) + k_f\left(\varphi_{s1}+\varphi_{s2}\right)\right)}\right]\right]$
$\nu_{hnf} = \dfrac{\dfrac{\mu_f}{[(1-\varphi_{s1})(1-\varphi_{s2})]^{2.5}}}{[(1-\varphi_{s2})\{(1-\varphi_{s1})\rho_f + \varphi_{s1}\rho_{s1}\} + \varphi_{s2}\rho_{s2}}$
$\dfrac{\nu_{hnf}}{\nu_{nf}} = \dfrac{\left[(1-\varphi)\rho_f + \varphi\rho_f\right](1-\varphi)^{2.5}}{[(1-\varphi_{s1})(1-\varphi_{s2})]^{2.5}\left[(1-\varphi_{s2})\left\{(1-\varphi_{s1})\rho_f + \varphi_{s1}\rho_{s1}\right\} + \varphi_{s2}\rho_{s2}\right.}$
$\dfrac{\alpha_{hnf}}{\alpha_f} = \dfrac{\left[\left(\dfrac{k_{s1}}{k_f}-2\right) - 2\varphi_{s1}\left(1-\dfrac{k_{s1}}{k_f}\right)\right]\left[\left(\dfrac{k_{s2}}{k_f}-2\right) - 2\varphi_{s2}\left(1-\dfrac{k_{s2}}{k_f}\right)\right]}{\left[\left(\dfrac{k_{s1}}{k_f}+2\right) - 2\varphi_{s1}\left(1-\dfrac{k_{s2}}{k_f}\right)\right]\left[\left(\dfrac{k_{s2}}{k_f}+2\right) + 2\varphi_{s2}\left(1-\dfrac{k_{s2}}{k_f}\right)\right]}$
$\times\left[(1-\varphi_{s2})\left\{(1-\varphi_{s1}) + \varphi_{s1}\dfrac{(\rho C_p)_{s1}}{(\rho C_p)_f}\right\} + \dfrac{\varphi_{s2}(\rho C_p)_{s2}}{(\rho C_p)_f}\right]$
$\dfrac{\sigma_{hnf}}{\sigma_f} = \dfrac{\left(\dfrac{\sigma_{s1}\varphi_{s1}+\sigma_{s2}\varphi_{s2}}{(\varphi_{s1}+\varphi_{s2})} + 2\sigma_f + 2\left(\sigma_{s1}\varphi_{s1}+\sigma_{s2}\varphi_{s2}\right) - 2\sigma_f\left(\varphi_{s1}+\varphi_{s2}\right)\right)}{\left(\dfrac{\sigma_{s1}\varphi_{s1}+\sigma_{s2}\varphi_{s2}}{(\varphi_{s1}+\varphi_{s2})} + 2\sigma_f - 2\left(\sigma_{s1}\varphi_{s1}+\sigma_{s2}\varphi_{s2}\right) + \sigma_f\left(\varphi_{s1}+\varphi_{s2}\right)\right)}$

Table 2: Thermo-physical characteristics of nano-materials and water of [22]

Thermal physical properties	Fluid phase (water)	Copper (Cu)	Silver (Ag)
$C_p\left(\dfrac{J}{kgK}\right)$	4179	385	235

(Continued)

Table 2 (continued)

Thermal physical properties	Fluid phase (water)	Copper (Cu)	Silver (Ag)
$\rho\left(\frac{kg}{m^3}\right)$	997.1	8933	10500
$k\left(\frac{W}{mK}\right)$	0.613	400	429
$\beta * 10^5$	21	1.67	1.89
σ	0.05	5.96×10^7	6.3×10^7

Table 3: Comparative values of $f''(y)$ when $M = 0.5$

β	$f''(y)$	
	Present results	Hayat et al. [22]
0.1	0.4154	0.4045
0.4	0.7321	0.7106
0.7	0.8751	0.8530

Table 4: We calculated this through maple

M Hartmann number	β Casson parameter	λ lubrication parameter	N index of lubrication	P_r Prandtl number	C_f	$\theta'(\eta)$
.4	2	.2		6.2	1.7546	
.5				6.2	1.6747	
.6					1.5851	
		.5			1.7546	
		.66			1.6986	
		.8			1.5970	
	.6				1.9141	
	.5				2.0375	
	.8				1.750	
.5			0.5		1.77646	.91152
.6			0.2		1.74056	.78914
.7			0.1		1.82999	.69193

5 Concluding Remarks

In the present investigation, water served as the acting base fluid, and we explored the MHD oblique-stagnation flow of a hybrid nanofluid into an oscillatory surface containing metal nanoparticles (Cu and Ag). Temperature T and the influence of the velocity distribution are additionally taken

into account. Numerical solutions of the governing equations are carried out utilising BVP [midrich] in Maple. After recognising the problem category (BVP) by itself. The velocity and temperature distributions of nanofluids are tested against various variables. Table 4 presents numerical data for skin friction and heat transfer efficiency. The significant results from our inquiry have been outlined below:

- Hartman number M is discussed in the graphs.
- $g'(\eta), \theta'(\eta)$ increases when Hartmann number M increases.
- Skin friction will decrease when it increases M.

The index of the parameter n will increase when we increase it M.

Acknowledgement: Authors Most respected Professor Dr. Sohail Nadeem and Dr. Nadeem Salamat are thankful to endless support.

Funding Statement: The authors received no specific funding for this study.

Author Contributions: The authors claim to have given the article their all throughout research. The PhD scholar Mirza Naveed Jahangeer Baig evaluated the piece of writing; all other authors, working under the direction of Professor Sohail Nadeem, checked and wrote it.

Availability of Data and Materials: No data was used for the research described in this article.

Conflicts of Interest: The authors declare that they have no conflicts of interest to report regarding the present study.

References

1. Masuda, H., Ebata, A., Teramae, K. (1993). Alteration of thermal conductivity and viscosity of liquid by dispersing ultra-fine particles. Dispersion of Al_2O_3, SiO_2 and TiO_2 ultra-fine particles. *Netsu Bussei, 7,* 227–233.
2. Choi, S. U., Eastman, J. A. (1995). *Enhancing thermal conductivity of fluids with nanoparticles (No. ANL/MSD/CP-84938; CONF-951135-29)*. Argonne, USA: Argonne National Lab (ANL).
3. Turgut, A., Elbasan, E. (2014). Nanofluids for electronics cooling. *2014 IEEE 20th International Symposium for Design and Technology in Electronic Packaging (SIITME)*, pp. 35–37. Bucharest, Romania. https://doi.org/10.1109/SIITME.2014.6966989
4. Hsieh, S. S., Leu, H. Y., Liu, H. H. (2015). Spray cooling characteristics of nanofluids for electronic power devices. *Nanoscale Research Letters, 10(1),* 1–16.
5. Riaz, A., Hassan, Q. M. U., Abbas, T., Ghachem, K., Majeed, A. et al. (2022). A study on effectiveness of the variational theory in fluid dynamics applications. *Alexandria Engineering Journal, 61(12),* 10779–10789.
6. Khan, U., Zaib, A., Ishak, A. (2021). Non-similarity solutions of radiative stagnation point flow of a hybrid nanofluid through a yawed cylinder with mixed convection. *Alexandria Engineering Journal, 60(6),* 5297–5309.
7. Acharya, N. (2021). Spectral quasi linearization simulation on the hydrothermal behavior of hybrid nanofluid spraying on an inclined spinning disk. *Partial Differential Equations in Applied Mathematics, 4,* 100094.
8. Suresh, S., Venkitaraj, K. P., Selvakumar, P., Chandrasekar, M. (2012). Effect of Al_2O_3-Cu/water hybrid nanofluid in heat transfer. *Experimental Thermal and Fluid Science, 38,* 54–60.

9. Weidman, P. D. (2012). Non-axisymmetric Homann stagnation-point flows. *Journal of Fluid Mechanics, 702,* 460–469.
10. Ur Rehman, F., Nadeem, S. (2018). Heat transfer analysis for three-dimensional stagnation-point flow of water-based nanofluid over an exponentially stretching surface. *Journal of Heat Transfer, 140(5),* 052401.
11. Yuan, B., Moghanloo, R. G. (2018). Nanofluid pre-treatment, an effective strategy to improve the performance of low salinity waterflooding. *Journal of Petroleum Science and Engineering, 165,* 978–991.
12. Anderson, J. L. (1989). Colloid transport by interfacial forces. *Annual Review of Fluid Mechanics, 21(1),* 61–99.
13. Abbasi, A., Farooq, W., Khan, S. U., Riaz, I. (2023). Lubricated surface oblique stagnation point flow of second-grade fluid with heat and mass transfer phenomenon: Applications to hydraulic systems. *Waves in Random and Complex Media,* 1–20. https://doi.org/10.1080/17455030.2022.2157513
14. Nadeem, S., Mehmood, R., Akbar, N. S. (2013). Non-orthogonal stagnation points flow of a nano non-Newtonian fluid towards a stretching surface with heat transfer. *International Journal of Heat and Mass Transfer, 57(2),* 679–689.
15. Wang, C. Y. (1990). Liquid film on an unsteady stretching surface. *Quarterly of Applied Mathematics, 48(4),* 601–610.
16. Zahor, F. A., Jain, R., Ali, A. O., Masanja, V. G. (2023). Modeling entropy generation of magnetohydrodynamics flow of nanofluid in a porous medium: A review. *International Journal of Numerical Methods for Heat & Fluid Flow, 33(2),* 751–771.
17. Kalpana, G., Madhura, K. R., Kudenatti, R. B. (2022). Numerical study on the combined effects of Brownian motion and thermophoresis on an unsteady magnetohydrodynamics nanofluid boundary layer flow. *Mathematics and Computers in Simulation, 200,* 78–96.
18. Sepehrnia, M., Khorasanizadeh, H., Shafii, M. B. (2021). Effect of transverse and parallel magnetic fields on thermal and thermo-hydraulic performances of ferro-nanofluid flow in trapezoidal microchannel heat sink. *International Journal of Numerical Methods for Heat & Fluid Flow, 31(7),* 2089–2111.
19. Khan, H., Ali, F., Khan, N., Khan, I., Mohamed, A. (2022). Electromagnetic flow of Casson nanofluid over a vertical riga plate with ramped wall conditions. *Frontiers in Physics, 10,* 1005447. https://doi.org/10.3389/fphy.2022.1005447
20. Rana, S., Mehmood, R., Akbar, N. S. (2016). Mixed convective oblique flow of a Casson fluid with partial slip, internal heating and homogeneous-heterogeneous reactions. *Journal of Molecular Liquids, 222,* 1010–1019.
21. Hayat, T., Nadeem, S., Khan, A. U. (2018). Rotating flow of Ag-CuO/H_2O hybrid nanofluid with radiation and partial slip boundary effects. *The European Physical Journal E, 41,* 1–9.
22. Hayat, T., Nadeem, S. (2017). Heat transfer enhancement with Ag-CuO/water hybrid nanofluid. *Results in Physics, 7,* 2317–2324.